

Single Impurity Problem in Iron-Pnictide Superconductors

Toshikaze KARIYADO^{1*} and Masao OGATA^{1,2}

¹*Department of Physics, University of Tokyo, 7-3-1 Hongo, Bunkyo, Tokyo 113-0033*

²*JST, TRIP, Sanbancho, Chiyoda, Tokyo 102-0075*

Single impurity problem in iron-pnictide superconductors is investigated by solving Bogoliubov-de Gennes (BdG) equation in the five-orbital model, which enables us to distinguish s_{+-} and s_{++} superconducting states. We construct a five-orbital model suitable to BdG analysis. This model reproduces the results of random phase approximation in the uniform case. Using this model, we study the local density of states around a non-magnetic impurity and discuss the bound-state peak structure, which can be used for distinguishing s_{+-} and s_{++} states. A bound state with nearly zero-energy is found for the impurity potential $I \sim 1.0$ eV, while the bound state peaks stick to the gap edge in the unitary limit. Novel multiple peak structure originated from the multi-orbital nature of the iron pnictides is also found.

KEYWORDS: iron pnictides, superconductivity, Bogoliubov-de Gennes equation, impurity

Much effort has been devoted to elucidate the structure of superconducting gap functions in the recently discovered iron pnictides.¹⁾ However, there are still many debates on this issue. Experimentally, the measurement of the quasi-particle interference pattern²⁾ and the existence of the half-integer flux-quantum transition³⁾ suggest that there is an internal π -phase shift of the gap function in iron-pnictide superconductors. Furthermore, nodal behaviors observed in some families of iron pnictides⁴⁾ indicate that the repulsive interaction plays important roles and the pairing with π -phase shift of the gap function sounds reasonable. On the other hand, it is claimed that the robustness against impurity doping cannot be consistent with the above mechanism.^{5,6)} Many theoretical studies have been performed in order to explain the high temperature superconductivity in iron pnictides.⁷⁻¹⁷⁾ Most of these theories have concluded that there exists inter-band sign reversal of the gap function (s_{+-} state). Recently, high temperature superconductivity without inter-band sign reversal (s_{++} state) is also suggested.¹⁷⁾ Considering these situations, it is important and urgent to develop some theories which enable us to distinguish the s_{+-} and s_{++} states. There have been several theoretical proposals for detecting the s_{+-} state. However, it is a difficult and subtle problem to distinguish s_{+-} and s_{++} state than to detect other unconventional superconducting states such as d-wave pairing, since the symmetries of the gap functions are the same for s_{+-} and s_{++} state.

In this paper, we investigate a single impurity problem since it can serve as a possible method to detect the sign change of the gap function. Actually, this problem has been discussed mainly in some simplified two band models for iron-pnictide superconductors.¹⁸⁻²⁵⁾ However, as we show here, detecting the s_{+-} state is subtle problem and the entangled nature of the multiple bands and the Fermi surface structure, which characterize iron pnictides, should be taken into account. In the first part of this paper, we construct a model which can be used in the

real-space single impurity problem. Although the five-orbital *Hubbard* model has been studied quite often, it is not suitable for our purpose since it does not give a superconducting ground state in the mean field theory. Here we construct a model whose interaction terms are chosen so as to reproduce the results in the five-orbital Hubbard model calculated within random phase approximation (RPA). The hopping integrals of this model are taken from the downfolded result. Then, the local density of states (LDOS) around a single non-magnetic impurity is calculated by solving Bogoliubov-de Gennes (BdG) equation for the obtained model. The results show clear formation of in-gap bound state, which turns out to be a good quantity for distinguishing s_{+-} and s_{++} states. We find that the dependence of the spectrum on the impurity potential strength is unique to the present system, and there are novel multiple peak structures in LDOS for a certain parameter range.

Now, we explain the five-orbital model used in this study. Hamiltonian for the used model can be written as

$$\begin{aligned} \mathcal{H} = & \sum_{\langle ij \rangle} \sum_{\sigma} \sum_{ab} t_{a,b;i,j} c_{ia\sigma}^{\dagger} c_{jb\sigma} + I \sum_{\sigma} \sum_a c_{r^*a\sigma}^{\dagger} c_{r^*a\sigma} \\ & + \sum_i \sum_{\sigma} \sum_{aba'b'} g_{aa'b'b}^{(0)} c_{ia\sigma}^{\dagger} c_{ib\bar{\sigma}}^{\dagger} c_{ia'\bar{\sigma}} c_{ib'\sigma} \\ & + \sum_{\langle\langle ij \rangle\rangle} \sum_{\sigma} \sum_{aba'b'} g_{aa'b'b}^{(1)} c_{ia\sigma}^{\dagger} c_{jb\bar{\sigma}}^{\dagger} c_{ja'\bar{\sigma}} c_{ib'\sigma} \\ & + \sum_{\langle\langle\langle ij \rangle\rangle\rangle} \sum_{\sigma} \sum_{aba'b'} g_{aa'b'b}^{(2)} c_{ia\sigma}^{\dagger} c_{jb\bar{\sigma}}^{\dagger} c_{ja'\bar{\sigma}} c_{ib'\sigma}, \end{aligned} \quad (1)$$

where r^* represents the position of the impurity site, and $\langle ij \rangle$ and $\langle\langle ij \rangle\rangle$ represent the nearest and next nearest neighbor pairs respectively. Indices a or b run through 0 to 4, where 0 to 4 correspond to $d_{3z^2-r^2}$, d_{zx} , d_{yz} , $d_{x^2-y^2}$, and d_{xy} orbitals in this order. Hopping integrals $t_{a,b;i,j}$ are same as those in the Table I of Kuroki *et al.*⁸⁾ For details of these hopping parameters, see Ref 8) and a brief description is also available in our previous paper.¹⁶⁾ The effect of impurity is simply treated as a local

*E-mail: kariyado@hosi.phys.s.u-tokyo.ac.jp

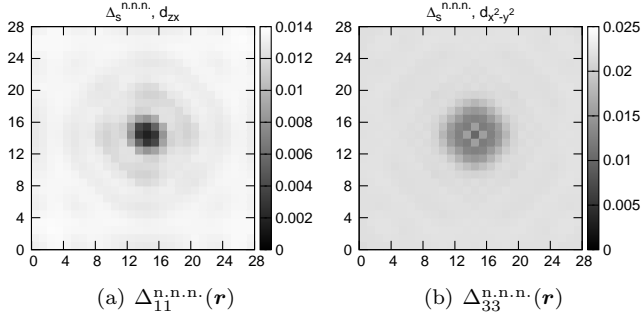


Fig. 1. Real space distribution of the order parameter $\Delta_{aa}^{n,n,n}(\mathbf{r})$ around the impurity site with $I = 1.0$ eV. (a) for the orbital 1 (d_{zx}) and (b) for the orbital 3 ($d_{x^2-y^2}$).¹⁶⁾

potential shift, I , in eq. (1). The orbital dependence of the potential shift and the long-range impurity effects are neglected here.

Coupling constants $g^{(i)}$ s in eq. (1) are chosen so as to reproduce the superconducting gap functions in the multi-orbital Hubbard model calculated within RPA.¹⁶⁾ It was shown that the gap function obtained in RPA can be well reproduced with short-range pairings up to the next nearest neighbor sites when it is written in the *orbital* representation, instead of the *band* representation. This point is reflected in eq. (1), where it is written in the orbital representation and the interaction terms are kept up to the next nearest neighbor sites. It was also shown that the pairings of $d_{3z^2-r^2}$ and d_{xy} orbitals are less important since the density of states (DOS) just around the Fermi energy mainly comes from $d_{zx/yz}$ and $d_{x^2-y^2}$ orbitals.¹⁶⁾ Furthermore, the inter-orbital pairings are less important than the intra-orbital ones in the s-wave channel. Based on these features, we have reduced the number of necessary parameters. Using the effective interaction calculated within RPA ($V_{abcd}^{\text{RPA}}(k)$, not shown), we obtain

$$g_{1111}^{(0)} = g_{2222}^{(0)} = g_{3333}^{(0)} = 3.0, \quad (2a)$$

$$g_{1111}^{(1)} = g_{2222}^{(1)} = g_{3333}^{(1)} = -0.75, \quad (2b)$$

$$g_{1111}^{(2)} = g_{2222}^{(2)} = g_{3333}^{(2)} = -0.27, \quad (2c)$$

$$g_{1221}^{(0)} = g_{1331}^{(0)} = g_{2332}^{(0)} = 0.3, \quad (2d)$$

$$g_{1221}^{(1)} = g_{1331}^{(1)} = g_{2332}^{(1)} = 0.075, \quad (2e)$$

$$g_{1221}^{(2)} = g_{1331}^{(2)} = g_{2332}^{(2)} = -0.027, \quad (2f)$$

in the unit of eV. Note that $g_{abba}^{(i)} = g_{baab}^{(i)}$ and parameters not shown here are set to be zero. $g_{aaaa}^{(0)}$ represents the onsite repulsion and $g_{aaaa}^{(1)}$ ($g_{aaaa}^{(2)}$) represents the effective attractive interaction between the nearest (next nearest) neighbor sites, mainly induced by the broad (π, π) (sharp near $(\pi, 0)$) peak in $V_{aaaa}^{\text{RPA}}(k)$.

Hamiltonian, eq. (1), is solved in the mean field approximation, where only the BCS type decomposition is used neglecting the Hartree-Fock type contribution. Order parameters are assumed to be site-dependent and then we obtain the multi-orbital version of the BdG equation. In actual calculations, we introduce the energy cut-

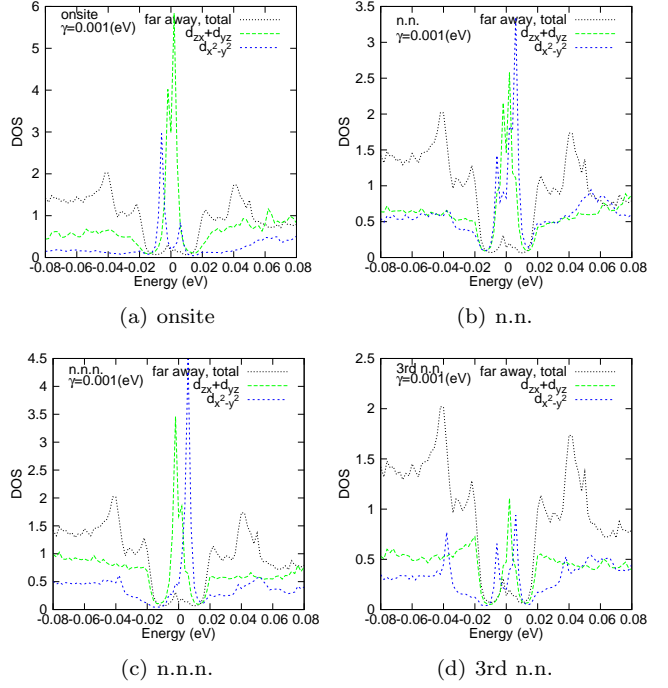


Fig. 2. Partial LDOS in the case of $I = 1.0$ eV on the several sites near the impurity. (a) shows partial LDOS at just on the impurity site, (b) on the nearest, (c) the next-nearest, and (d) the third-nearest-neighbor site, respectively. Lines in each figure represent $\rho_1(\mathbf{r}, \omega) + \rho_2(\mathbf{r}, \omega)$ (sum of the contributions from d_{zx} and d_{yz} orbitals) and $\rho_3(\mathbf{r}, \omega)$ (contribution from $d_{x^2-y^2}$ orbital). LDOS at a site far from the impurity is also plotted.

off, ω_c , necessary in the standard BCS theory, i.e., we assume that the pairing occurs only between the electrons with energies ε satisfying $|\varepsilon - \mu| < \omega_c$, where μ is the chemical potential. Throughout this paper, we use $\omega_c = 0.1$ eV. This choice of ω_c does not affect the following discussion. We solve the BdG equation in the lattices up to 28×28 sites with an impurity at the center, and determine the site-dependent order parameters by iteration. The electron number is fixed at $n = 6.1$ by adjusting the chemical potential, μ . In order to calculate physical quantities, such as LDOS, we use the “super-cell” method²⁶⁾ to improve the numerical accuracy. In this “super-cell” method, the 28×28 lattice with an impurity is treated as a “unit cell” and the whole system is composed of 13×13 repetition of this unit cell. The connection between the unit cells is represented by the wave vectors $\mathbf{k} = (2\pi n_x/13, 2\pi n_y/13)$. The LDOS in this “super-cell” method is given by

$$\rho(\mathbf{r}, \omega) = \sum_a \rho_a(\mathbf{r}, \omega), \quad (3)$$

$$\rho_a(\mathbf{r}, \omega) = -\frac{1}{\pi} \sum_{\mathbf{k}} \text{Im} G_{\mathbf{r}a, \mathbf{r}a}^R(\mathbf{k}, \omega) \quad (4)$$

where $\rho_a(\mathbf{r}, \omega)$ is the partial LDOS for the orbital a , and $G_{\mathbf{r}a, \mathbf{r}'a}^R(\mathbf{k}, \omega)$ is the retarded Green’s function in real space for the lattice sites \mathbf{r} and \mathbf{r}' in the unit cell. In following figures, the Dirac delta functions in the LDOS are replaced by the lorentzian function with the half width $\gamma = 0.001$ eV.

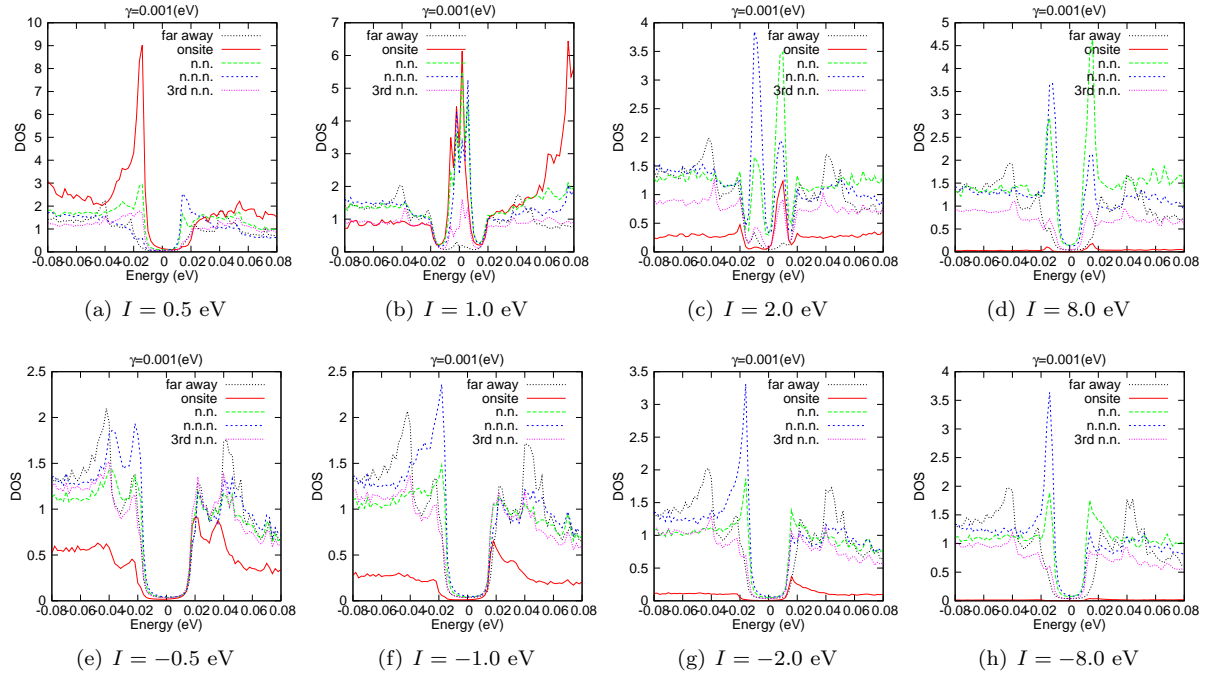


Fig. 3. LDOS for various impurity potential I . Lines in each figure represents LDOS at the site far from the impurity site, on the impurity site, nearest neighbor site, next nearest neighbor site, and 3rd nearest neighbor site.

Figure 1 shows the obtained order parameter and its modulation around the impurity site. Here, we consider the case of $I = 1.0$ eV. A representative order parameter, $\Delta_{aa}^{n.n.n.}(\mathbf{r})$, defined as

$$\Delta_{aa}^{n.n.n.}(\mathbf{r}) \equiv \sum_{\mathbf{r}'}' \Delta_{\mathbf{r}'a, \mathbf{r}a} = \sum_{\mathbf{r}'}' \sum_{a'} g_{aa'a'a}^{(2)} \langle c_{\mathbf{r}'a'\sigma}^\dagger c_{\mathbf{r}a'\sigma}^\dagger \rangle, \quad (5)$$

is plotted in Fig. 1. Here, $\sum_{\mathbf{r}'}'$ means that the summation over the next nearest neighbor sites of \mathbf{r} . The amplitude of $\Delta_{aa}^{n.n.n.}(\mathbf{r})$ is suppressed near the impurity and we can estimate the coherence length to be about four or five lattice spacing. At a site far away from the impurity, where the bulk behaviors are expected, we have $\Delta_{11}^{n.n.n.}/\Delta_{33}^{n.n.} \sim -0.41$, $\Delta_{11}^{n.n.n.}/\Delta_{33}^{n.n.} \sim -0.30$, $\Delta_{33}^{\text{onsite}}/4\Delta_{33}^{n.n.} \sim 0.54$, and $\Delta_{33}^{n.n.n.}/\Delta_{33}^{n.n.} \sim -0.50$. Roughly speaking, these ratios are consistent with those obtained in RPA for $n = 6.1$ and $J_H/U = 0.2$.¹⁶⁾ Although the value of $\Delta_{11}^{n.n.n.}/\Delta_{33}^{n.n.}$ is slightly overestimated compared with RPA, the present result captures most of the features of RPA result. $\Delta_{aa}^{n.n.}(\mathbf{r})$, which is defined for the nearest-neighbor sites, shows a similar behavior as $\Delta_{aa}^{n.n.n.}(\mathbf{r})$, while $\Delta_{aa}^{\text{onsite}}(\mathbf{r}) \equiv \Delta_{\mathbf{r}a, \mathbf{r}a}$ shows an overshooting behavior, i.e., it exceeds the bulk value at some points around the impurity.

Next, we show LDOS around the impurity for the case of $I = 1.0$ eV in Fig. 2. In each figure, the partial LDOS for $d_{zx/yz}$ and $d_{x^2-y^2}$ orbitals are plotted. From Figs. 2(a)-2(c), we can see the clear formation of the impurity induced in-gap bound state around impurity. When we look at the obtained spectrum more closely, we find that the peaks appear as a pair, i.e., at $\pm E$ for each orbital, and that the width of each pair, E , depends on the orbital. As a result, total LDOS, which is the sum of the partial LDOS, shows novel multiple peak struc-

tures (see also Fig. 3(b)). This feature is characteristic in iron pnictides and can be captured only in our realistic five-orbital model. At the third nearest neighbor site (Fig. 2(d)), on the other hand, the in-gap bound state peaks become small and the bulk-like coherence peaks recover.

Impurity potential dependence of the LDOS is summarized in Fig. 3 where the results for I ranging from -8.0 eV to $+8.0$ eV are shown. In each figure, we plot LDOS at several sites around the impurity up to third nearest neighbor site as well as LDOS far away from the impurity. As a function of I ($I > 0$), (Fig. 3(a-d)), we find that the bound state appears at the edge of the gap ($I = 0.5$ eV), and moves toward nearly zero energy ($I = 1.0$ eV), and then, goes back to the gap edge ($I = 2.0$ eV and $I = 8.0$ eV). As a result, the bound state formation is most prominent at $I = 1.0$ eV. On the other hand, when I is negative, (Fig. 3(e-h)), the bound-state energies stick to the gap edge and do not approach the zero energy. In this case, the amplitude of the peak just grows with increasing $|I|$. Comparing these cases, we can see that the impurity with negative I has much less effects than the impurity with positive I when $|I|$ is relatively small. In contrast, when $|I|$ is large and in the unitary limit, LDOS structures are similar for both positive and negative I 's. This is reasonable since the impurity with large $|I|$ works as a site onto which electrons cannot hop, whichever the sign of I is.

Experimentally, LDOS can be measured by scanning tunneling microscopy/spectroscopy (STM/STS). Since the in-gap bound state around a non-magnetic impurity does not appear in s_{++} state, the bound state formation discussed above can be used to distinguish s_{+-} and s_{++} state. In particular, if the impurity potential is around

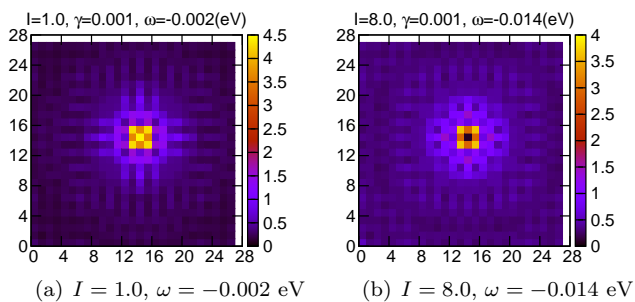


Fig. 4. Real space map of LDOS for (a) $I = 1.0$, $\omega = -0.002$ eV and (b) $I = 8.0$, $\omega = -0.014$ eV.

$I \sim 1.0$ eV, the difference between s_{+-} and s_{++} states becomes most prominent since the in-gap bound state appears at the near zero-energy and the peak is very large. Even if the large in-gap state is not observed, the spectrum at the gap edge can be carefully investigated to distinguish the s_{+-} and s_{++} state. Up to now, the superconducting gap has been successfully observed in Fe(TeSe) system,^{2,27)} and the detailed comparison of the theory and experiments is an interesting future work.

We plot the real space map of LDOS in Fig. 4. In order to see the typical behavior of the impurity induced bound states, we choose the two cases with (a) $I = 1.0$ eV, $\omega = -0.002$ eV and (b) $I = 8.0$ eV, $\omega = -0.014$ eV, in which the bound state peaks in LDOS are clearly seen. For both cases, we find that the real space distribution of LDOS or the extension of the bound state is nearly isotropic. This will be due to the following two reasons: 1) Fermi surfaces of the used model are circular, and 2) the obtained gap function is nodeless in the bulk limit, which means that there is no special direction associated with the node. This feature will be changed if we consider a parameter region where the nodal gap function is obtained, or if the square Fermi surfaces appear.

Here, we discuss the obtained results in connection to the T -matrix approximation, which has been used to study the formation of the bound state in the superconducting state.^{28,29)} This approximation applied on the similar five orbital model gives the results consistent with the present paper,⁶⁾ although the site-resolved information is difficult to obtain in the T -matrix approximation. We discuss the following two points. One is about the I dependence of the spectrum, which is understood from the particle-hole asymmetry of DOS in the present model. To be more specific, the DOS has larger weight below the Fermi energy than above the Fermi energy. We can show that this asymmetry results in the formation of the nearly zero-energy bound state when I is small and positive. (Details will be published elsewhere.) For other values of I , we can show similarly that the bound states are formed at the gap edge. The second point is about the multiple peak structure found in the case of $I = 1.0$ eV. In this case, we can show that the T -matrix can be block diagonalized with each block having only intra-orbital contribution. This means that each orbital can sustain the bound state independently, and this is the origin of the multiple peak structure.

It is tempting to speculate that the present results are connected to the experimentally observed robustness against the impurity doping. Namely, the impurity effect is weak when I is negative and small, which may explain the robustness against the impurity doping, although the magnitude of I and the relation to the residual resistivity should be taken account of carefully.⁶⁾

In summary, we have calculated the LDOS around a non-magnetic impurity in the effective model for iron-pnictide superconductors. The model used here has realistic band structure and the effective interaction is determined so as to reproduce the RPA results of the gap function. It has been shown that the observation of the in-gap bound state enables us to distinguish the s_{++} and s_{+-} states. An impurity with $I \sim 1.0$ eV gives large low energy peak, and we have also shown that the bound state peak appears at just below (or above) the gap edge in the unitary limit. An impurity with negative and small I has relatively small effects on LDOS. The modeling of the case having the nodal gap function and of the recently proposed phonon-assisted orbital-fluctuation-mediated superconductivity are interesting extensions of the present study. Similar analysis on the quasi-particle interference patterns would also give important information.

Acknowledgment

We thank K. Kuroki, H. Ikeda, K. Nakamura, and T. Hanaguri for stimulating discussion. T.K. is supported by JSPS Research Fellowship.

- 1) K. Ishida, Y. Nakai, and H. Hosono: J. Phys. Soc. Jpn. **78** (2009) 062001.
- 2) T. Hanaguri, S. Niitaka, K. Kuroki, and H. Takagi: Science **328** (2010) 474.
- 3) C.-T. Chen, C. C. Tsuei, M. B. Ketchen, Z.-A. Ren, and Z. X. Zhao: Nature Physics **6** (2010) 260.
- 4) K. Hashimoto, M. Yamashita, S. Kasahara, Y. Senshu, N. Nakata, S. Tonegawa, K. Ikada, A. Serafin, A. Carrington, T. Terashima, H. Ikeda, T. Shibauchi, and Y. Matsuda: arXiv:0907.4399.
- 5) M. Sato, Y. Kobayashi, S. C. Lee, H. Takahashi, E. Satomi, and Y. Miura: J. Phys. Soc. Jpn. **79** (2010) 014710.
- 6) S. Onari and H. Kontani: Phys. Rev. Lett. **103** (2009) 177001.
- 7) I. Mazin, D. Singh, M. Johannes, and M. Du: Phys. Rev. Lett. **101** (2008) 057003.
- 8) K. Kuroki, S. Onari, R. Arita, H. Usui, Y. Tanaka, H. Kontani, and H. Aoki: Phys. Rev. Lett. **101** (2008) 087004.
- 9) A. V. Chubukov, D. Efremov, and I. Eremin: Phys. Rev. B **78** (2008) 134512.
- 10) Y. Yanagi, Y. Yamakawa, and Y. Ōno: J. Phys. Soc. Jpn. **77** (2008) 123701.
- 11) H. Ikeda: J. Phys. Soc. Jpn. **77** (2008) 123707.
- 12) Y. Fuseya, T. Kariyado, and M. Ogata: J. Phys. Soc. Jpn. **78** (2009) 023703.
- 13) V. Cvetkovic and Z. Tesanovic: Europhys. Lett. **85** (2009) 37002.
- 14) S. Graser, T. A. Maier, P. J. Hirschfeld, and D. J. Scalapino: New J. Phys. **11** (2009) 025016.
- 15) T. Nomura: J. Phys. Soc. Jpn. **78** (2009) 034716.
- 16) T. Kariyado and M. Ogata: J. Phys. Soc. Jpn. **79** (2010) 033703.
- 17) H. Kontani and S. Onari: Phys. Rev. Lett. **104** (2010) 157001.
- 18) Y. Bang, H.-Y. Choi, and H. Won: Phys. Rev. B **79** (2009) 054529.
- 19) M. Matsumoto, M. Koga, and H. Kusunose: J. Phys. Soc. Jpn. **78** (2009) 084718.

-
- 20) W.-F. Tsai, Y.-Y. Zhang, C. Fang, and J. Hu: Phys. Rev. B **80** (2009) 064513.
- 21) T. Ng and Y. Avishai: Phys. Rev. B **80** (2009) 104504.
- 22) J. Li and Y. Wang: Europhys. Lett. **88** (2009) 17009.
- 23) D. Zhang: Phys. Rev. Lett. **103** (2009) 186402.
- 24) A. Akbari, I. Eremin, and P. Thalmeier: Phys. Rev. B **81** (2010) 014524.
- 25) T. Zhou, X. Hu, J.-X. Zhu, and C. S. Ting: arXiv:0904.4273.
- 26) A. Himeda, M. Ogata, Y. Tanaka, and S. Kashiwaya: J. Phys. Soc. Jpn. **66** (1997) 3367.
- 27) T. Kato, Y. Mizuguchi, H. Nakamura, T. Machida, H. Sakata, and Y. Takano: Phys. Rev. B **80** (2009) 180507.
- 28) H. Shiba: Prog. Theor. Phys. **40** (1968) 435.
- 29) A. V. Balatsky, I. Vekhter, and J.-X. Zhu: Rev. Mod. Phys. **78** (2006) 373.